Available online at www.sciencedirect.com
ScienceDirect
Catalysis Today 127 (2007) 139–147
CATALYSIS TODAY
www.elsevier.com/locate/cattod

Support effects on structure and activity of molybdenum oxide catalysts for the oxidative dehydrogenation of ethane

George Tsilomelekis, Antonios Christodoulakis, Soghomon Boghosian *

Department of Chemical Engineering, University of Patras and Institute of Chemical Engineering and High Temperature Chemical Processes, Foundation of Research and Technology-Hellas (FORTH/ICE-HT), 26500 Patras, Greece

Available online 26 April 2007

Abstract

The structural and catalytic properties of MoO_3 catalysts supported on ZrO_2, Al_2O_3, TiO_2 and SiO_2 with Mo surface densities, n_s, in the range of 0.5–18.5 Mo/nm^2 were studied for the oxidative dehydrogenation (ODH) of ethane by *in situ* Raman spectroscopy and catalytic activity measurements at temperatures of 400–540 °C. The molecular structure of the dispersed surface species evolves from isolated monomolybdates (MoO_4 and MoO_5, depending on the support) at low loadings to associated MoO_x units in polymolybdate chains at high loadings and ultimately to bulk crystalline phases for loadings exceeding the monolayer coverage of the supports used. The nature of the oxide support material and of the Mo–O–support bond has a significant influence on the catalytic behaviour of the molybdena catalysts with monolayer coverage. The dependence of reactivity on the support follows the order $ZrO_2 > Al_2O_3 > TiO_2 > SiO_2$. The oxygen site involved in the anchoring Mo–O–support is of relevance for the catalytic activity.

Keywords: Supported molybdena catalysts; Support effect; Ethane ODH; Molecular structure; Molybdena active sites; *In situ* Raman spectra; Anchoring bonds; Support cation elecronegativity

1. Introduction

The need for light olefins remains an important challenge for the petrochemical industry. The catalytic dehydrogenation of alkanes either by direct dehydrogenation (DH) [1] or oxidative dehydrogenation (ODH) [2] is an attractive route for the synthesis of the corresponding alkenes, resulting in comparable yields in olefins. However, the thermodynamic feasibility of the ODH process has led to extensive evaluation of supported metal oxide catalysts, particularly for the ODH of propane and ethane. Supported vanadia [3–5] and molybdena [3,6–11] catalysts have been studied widely with a view to achieve high alkene yields, particularly in high alkane conversions.

Supported molybdena catalysts are among the most effective ones for the ODH of ethane [3,8,11], although their performance is generally inferior to vanadia-based catalysts [3,4]. It has been established that the process follows a Mars–van Krevelen mechanism involving breaking of a C–H bond as a slow step and participation of lattice oxygen. The efficiency of supported molybdena for activating the alkane C–H bond for the selective production of alkene is directly related to a number of factors including *inter alia*: (i) the surface composition; (ii) the local structure and the distribution of the dispersed MoO_x species; (iii) the nature and identity of the substrate/carrier; (iv) the molybdena phase loading; (v) parameters related to catalyst preparation procedures. Aspects related to the dispersion of molybdena on the support, the distribution of isolated and polymeric units as well as the structural characteristics of surface metal oxide groups can be studied by *in situ* Raman spectroscopy, which is a valuable method for probing the vibrational properties of metal–oxygen bonds [12–14]. The structures of supported MoO_3 catalysts have been studied extensively, mainly by *in situ* Raman spectroscopy in dehydrated conditions with most of the studies pertaining to Al_2O_3-supported catalysts [15]. The structure of the dispersed molybdena phase evolves from isolated MoO_x to two-dimensional chain-like oligomers involving Mo–O–Mo bridges and – at loadings exceeding monolayer coverage – crystalline MoO_3 or mixed metal oxide

* Corresponding author. Tel.: +30 2610 969557.
E-mail address: bogosian@iceht.forth.gr (S. Boghosian).

0920-5861/$ – see front matter © 2007 Elsevier B.V. All rights reserved.
doi:10.1016/j.cattod.2007.03.026

crystals (e.g. $Al_2(MoO_4)_3$ [11], $Zr(MoO_4)_2$ [16]). Both dioxo (tetracoordinated, CN = 4) and monooxo tetragonal pyramidic (CN = 5) configurations have been proposed for the isolated surface MoO_x species on Al_2O_3 [11,15] and SiO_2 [15], whereas monooxo tetragonal pyramidic configurations, O = Mo(–O–M)$_4$ (M = support metal atom) have been proposed for ZrO_2 [16,17] and TiO_2 [18]. Octahedral configurations with penta- and hexa-coordinated Mo atoms have been proposed for the dispersed $(MoO_x)_n$ polymeric domains on Al_2O_3 and ZrO_2 [11,15–17]; the configuration of polymolybdates is under dispute for SiO_2-supported catalysts with, e.g. postulations of geometries intermediate to tetrahedral and octahedral [18]. Structure–function relationships for the ODH of light alkanes remain scarce.

The molecular structure of a catalytic material is not static, but transforms readily by responding to changes in the atmosphere and in the conditions surrounding the catalyst material. The urge for knowledge-based understanding of the catalyst performance and for deriving structure–function relationships has led to the development of multi-operational spectroscopic reactor cells [1] enabling catalyst monitoring with simultaneous product analysis under actual reaction conditions (*operando* spectroscopy [19,20]).

The present study focuses on the effects of support (ZrO_2, Al_2O_3, TiO_2 and SiO_2) on the structure and catalytic behaviour of supported MoO_3 catalysts for the ODH of ethane by means of *in situ* Raman spectroscopy at temperatures of 400–550 °C with simultaneous catalytic measurements on the *same* sample. The effect of catalyst loading, temperature and reactant residence time on both Raman spectra and catalyst performance was studied. Emphasis was given in the exploration of the support effect by comparing the structures and functions for catalysts with monolayer coverage.

2. Experimental

2.1. Catalyst preparation and characterisation

The catalysts were prepared by wet impregnation of the support materials [ZrO_2 (Norton, 55 m^2/g); γ-Al_2O_3 (Engelhard, 183.9 m^2/g); TiO_2 (Alfa, 127 m^2/g); and SiO_2 (Alfa, 90.2 m^2/g)] using aqueous solutions (pH 4–5) of $(NH_4)_6Mo_7O_{24}{\cdot}4H_2O$ (Alfa). The solutions, of which the concentrations were adjusted so to correspond to the desired MoO_3 wt%, were subjected to rotation at 40–45 °C for 0.5–1 h and then to rotary evaporation at 45–70 °C under reduced pressure for 1.5 h in order to remove the solvent. Afterwards they were dried overnight at 100–140 °C and calcined in air in a muffle furnace. Finally, the calcined catalysts powders were sieved in order to obtain particle sizes in the range of 125–180 μm.

Surface areas were measured by N_2 adsorption using a Micromeritics Gemini II 2370 analyzer and standard multipoint BET analysis methods. Samples were evacuated for 2 h before N_2 adsorption measurements. Powder X-ray diffraction patterns were obtained at room temperature using a Philips PW 1830 diffractometer and Cu Kα radiation. The catalyst characteristics are summarized in Table 1. The samples are denoted by *x*Mo*M*, *x* being the wt% MoO_3 loading and *M* the support metal atom.

2.2. In situ Raman spectroscopy with simultaneous GC analysis

The home made *in situ* Raman cell used for the simultaneous monitoring of Raman spectra and catalytic activity of the studied catalysts has been described in Ref. [11]. The reactor cell, which had a gas inlet and outlet as well as an entrance to accommodate a thermocouple sheath was made of quartz

Table 1
Properties of the catalysts

Catalyst	wt% MoO_3	Calcination	S.A. (m^2/g)	Surface density (Mo/nm^2)	Crystalline phases
2MoZr	2	600 °C/4 h	48.7	1.7	ZrO_2 (monoclinic)
4MoZr	4	600 °C/4 h	44.3	3.8	ZrO_2 (monoclinic)
5.5MoZr	5.5	600 °C/4 h	44.7	5.2	ZrO_2 (monoclinic)
7MoZr	7	600 °C/4 h	40.9	7.2	ZrO_2 (monoclinic)
10MoZr	10	600 °C/4 h	40.0	10.5	ZrO_2, $Zr(MoO_4)_2$
5MoAl	5	650 °C/6 h	185.7	1.1	γ-Al_2O_3
10MoAl	10	650 °C/6 h	178.2	2.3	γ-Al_2O_3
15MoAl	15	650 °C/6 h	160.8	3.9	γ-Al_2O_3
20MoAl	20	650 °C/6 h	124.0	6.7	γ-Al_2O_3, $Al_2(MoO_4)_3$
30MoAl	30	650 °C/6 h	100.2	12.5	γ-Al_2O_3, $Al_2(MoO_4)_3$
3MoTi	3	480 °C/4 h	88.3	1.4	TiO_2 (anatase)
6MoTi	6	480 °C/4 h	101.3	2.5	TiO_2 (anatase)
9MoTi	9	480 °C/4 h	98.7	3.8	TiO_2 (anatase)
15MoTi	15	480 °C/4 h	109.1	5.8	TiO_2 (anatase)
21MoTi	21	480 °C/4 h	98.6	8.9	TiO_2, MoO_3
35MoTi	35	480 °C/4 h	79.2	18.5	TiO_2, MoO_3
1MoSi	1	550 °C/5 h	86.6	0.5	SiO_2
2MoSi	2	550 °C/5 h	81.4	1.0	SiO_2
7MoSi	7	550 °C/5 h	75.7	3.9	SiO_2, MoO_3

tubing (6 mm o.d.; 4 mm i.d. and 10 mm o.d.; 8 mm i.d. for the central larger part) and had a quartz frit for holding the catalysts in place in a fixed bed. The cell was mounted in vertical position inside a double walled quartz-glass transparent tube furnace mounted on a *xyz* plate that enabled its positioning on the optical table. The inner furnace tube is kanthal wire-wound for heating the reactor. Temperature was controlled and measured by a thermocouple inserted in the quartz sheath in contact with the catalyst bed.

The 488.0 and 514.5 nm lines of a Spectra Physics Stabilite 2017 Ar^+ laser were used for recording of the Raman spectra. The incident light (operated at a 30 mW power level at the sample) was focused on the catalyst bed by a slightly defocused lens, in order to reduce sample irradiance. The scattered light was collected at 90° (horizontal scattering plane), analyzed with a 0.85 Spex 1403 double spectrometer and detected by a −20 °C cooled RCA PMT equipped with EG&G photon counting electronics.

In situ Raman spectra under oxidizing conditions were recorded at temperatures 420–540 °C under flowing O_2 (99.999%) at a 15 cm^3/min flow rate. Catalysts supported on TiO_2 (anatase) were not treated above 500 °C in order to avoid phase transformations of the support. Prior to recording of the spectra, catalysts were held for at least 1 h under O_2 flow to ensure full oxidation. For the *operando* Raman–GC measurements during steady state ethane ODH conditions, a flow of a reactant gas mixture consisting of 5.6% C_2H_6/5.6% O_2 balanced in He was switched on right after treatment in O_2 at 550 °C. Each catalyst sample was examined at a range of reactant residence times such that the reactor operation conditions could be considered as differential. The residence time is expressed by the ratio *W*/*F* (*W*, catalyst weight in the range of 150–350 mg; *F*, total gas flow in the range of 20–200 cm^3/min). Comparisons of catalyst performances were done at $W/F = 0.28$ g s/cm^3 at temperatures in the range of 420–540 °C. The effect of residence time on catalytic activity was then explored at each temperature by varying either the catalyst weight or the total flow rate resulting in *W*/*F* values in the range 0.05–1 g s/cm^3. Before changing the operating temperature or the bed residence time (*W*/*F*) each sample was reoxidised under flowing O_2 at 550 °C in order to reinstate the initial surface composition. All gas flow rates were controlled by electronic mass flow meters.

The reactor effluent was analyzed by on-line GC (Schimadju 14B) using two packed columns (Porapak Q and Molecular Sieve 5A) in a series or bypass configuration and a thermal conductivity detector (TCD). Blank runs with no catalyst in bed were also performed in order to check the case of gas phase reaction contributions. Ethane conversion was less than 1% at 540 °C.

3. Results and discussion

3.1. Surface area and XRD

Table 1 summarises the basic characteristics of the catalyst samples. The deposition of molybdena results in a gradual decrease of the specific surface area, which in the case of TiO_2-supported samples is not monotonic. This can be attributed to blocking of support pores as larger MoO_x domains grow in the surface and to formation of crystalline phases, when monolayer coverage has been exceeded. The behaviour of the *x*MoTi samples is discussed below in the section pertaining to their respective *in situ* Raman spectra.

The XRD patterns (not shown for brevity) for the freshly calcined catalysts with low loadings indicate a fine dispersion of molybdena on the support (no peaks except for those of the respective supports are observed, see Table 1). To the contrary, for samples with high loadings additional weak diffraction lines, characteristic of crystalline phases are observed. These include either mixed metal oxide crystals [$Zr(MoO_4)_2$ and $Al_2(MoO_4)_3$] or crystalline MoO_3 (for TiO_2 and SiO_2 supported catalysts). These results are further supported by the Raman study described below. Raman spectroscopy is additionally able to detect crystalline nanoparticles for samples with loadings close to a monolayer that do not exhibit diffraction lines in the XRD spectra (e.g. 7MoZr, 15MoTi); most commonly such nanoparticles are dispersed on the surface following few ODH reaction cycles. The Mo surface density, n_s, corresponding to the polymolybdate saturation capacity on several metal oxide supports has been reported to be ∼5 Mo/nm^2 according to a number of experimental methods ([16] and references therein). The calculated theoretical monolayer coverage based on the effective ionic diameter of MoO_6 octahedra is 4.9 Mo/nm^2 [21], while molybdena monolayers of tetrahedral and octahedral coordination for loadings of up to 7 Mo/nm^2 have also been reported [22]. For the case of SiO_2-supported catalysts, the experimentally determined monolayer is around or less that 1 Mo/nm^2.

3.2. In situ Raman spectra of supported molybdena catalysts under O_2

The Raman spectra of dispersed surface molybdenum oxide species under dehydrated conditions exhibit bands that can give information on the vibrational properties of terminal Mo=O and bridging Mo–O–Mo functionalities. Furthermore, they exhibit features which are dependent on molybdena loading and temperature [11]. However, the occurrence of a distribution of chemical environments and strains within the dispersed MoO_x species makes it difficult to ascertain the coordination and the local structure around the Mo atom, particularly due to unavailability of surface molybdate reference compounds. Comparison to model compounds of known structure can be used more efficiently for band assignments of isolated (monomeric) surface species.

As examples, we will discuss briefly the Raman spectra obtained under O_2 flow at 450 °C for MoO_3/ZrO_2 and MoO_3/TiO_2 catalysts, shown in Figs. 1 and 2. The Raman spectra of MoO_3/Al_2O_3 have been described recently [11], whereas the surface distribution of mono- and polymolybdates on SiO_2 is in dispute [18] and will be addressed briefly below, in the context of the discussion pertaining to Raman spectra of monolayer catalysts. The strong band observed in spectra of all catalysts at

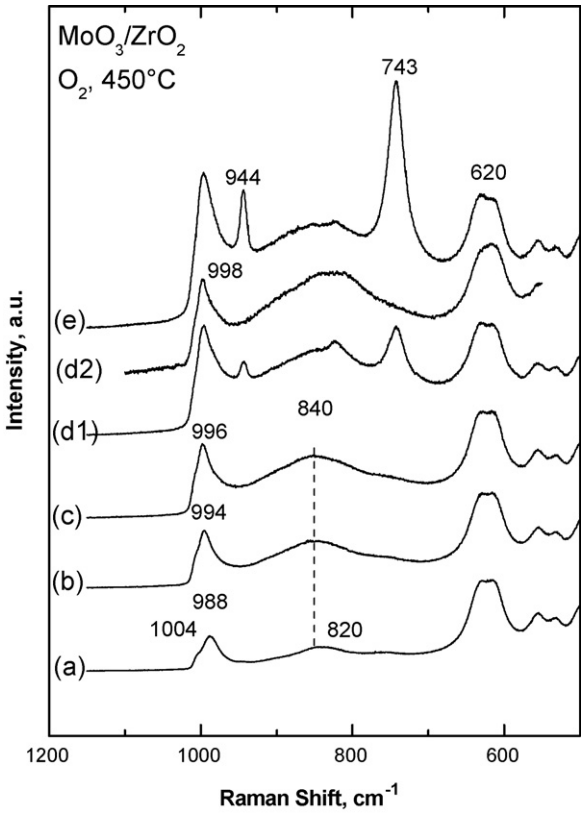

Fig. 1. *In situ* Raman spectra of MoO_3/ZrO_2 catalysts obtained under flowing O_2 at 450 °C: (a) 2MoZr; (b) 4MoZr; (c) 5.5MoZr; (d1) 7MoZr, fresh; (d2) 7MoZr, treated; (e) 10MoZr. Laser wavelength, $\lambda_0 = 488.0$ nm; laser power, $w = 30$ mW; scan rate, sr = 0.1–0.2 cm^{-1}/s; time constant, $\tau = 1$–2 s; spectral slit width, ssw = 8 cm^{-1}.

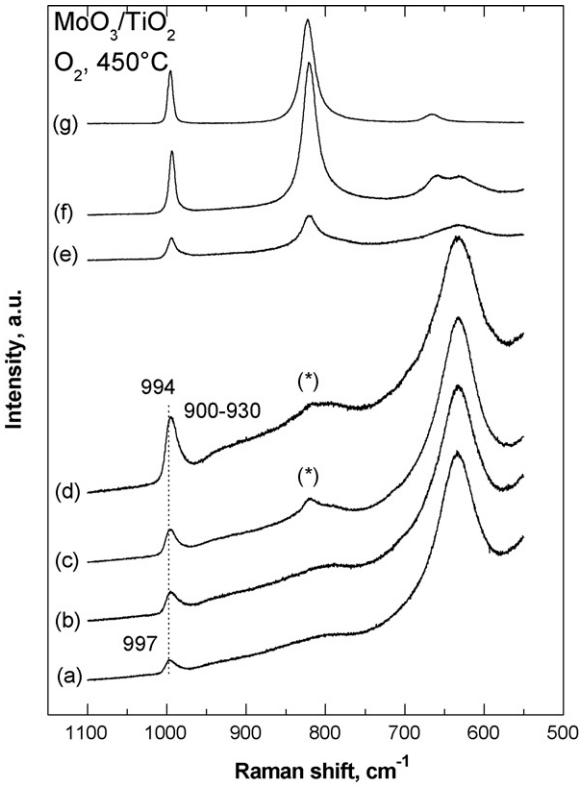

Fig. 2. *In situ* Raman spectra of MoO_3/TiO_2 catalysts obtained under flowing O_2 at 450 °C: (a) 3MoTi; (b) 6MoTi; (c) 9MoTi; (d) 15MoTi; (e) 21MoTi; (f) 35MoTi; (g) MoO_3. Laser wavelength, $\lambda_0 = 514.5$ nm; recording parameters: see Fig. 1 caption.

~620 cm^{-1} (Fig. 1a–e) is due to the monoclinic ZrO_2 support; all spectra in Fig. 1 are normalised relative to this band. With increasing Mo surface density, n_s, the progressive coverage of the support surface with Mo species leads to an increase in the relative intensity of the emerging bands that are due to MoO_x as compared to the 620 cm^{-1} ZrO_2 band. For the 2MoZr catalyst with surface density $n_s = 1.7$ Mo/nm^2 (spectrum a), bands due to dispersed surface molybdena are observed at 820–840 (broad), 988 (well defined) and ~1004 cm^{-1} (shoulder). With increasing loading (spectra b and c obtained for samples with n_s of 3.8 and 5.2 Mo/nm^2) the following are observed: (a) the 988 cm^{-1} band increases in intensity and undergoes a blue shift (996 cm^{-1} in spectrum c in Fig. 2); (b) the 1004 cm^{-1} is gradually being obscured under the wing of the 996 cm^{-1} band; (c) the broad 820–840 cm^{-1} band increases and is blue shifted due to domination of its high frequency component. For the 7MoZr and 10MoZr samples (spectra d1 and e) with n_s of 7.2 and 10.5 Mo/nm^2, one can observe traces of undispersed MoO_3 (presumably arising from nanoparticles not detectable by XRD) with characteristic weak feature at 822 cm^{-1} and increasing amounts of $Zr(MoO_4)_2$ (characteristic bands at 743 and 944 cm^{-1}). It should be pointed out that, following subjection to few ethane ODH reaction cycles, the crystalline phases present on the surface of the 7MoZr sample (spectrum d1 in Fig. 1) are completely dispersed (spectrum d2 obtained following few reaction cycles at 540 °C).

Previously, it has been shown (by means of oxygen isotopic exchange experiments) that dispersed molybdena occur as monooxo species on ZrO_2 [17]. Therefore, we proceed with spectral band assignments and proposals for plausible configurations for surface MoO_x species as follows. The bands at 1004 and 820 cm^{-1} (prevailing in spectrum a, Fig. 1) are assigned to the ν(Mo=O) and antisymmetric ν(O–Mo–O) modes of a surface mono-oxo isolated O = Mo(–O–Zr)$_4$ species

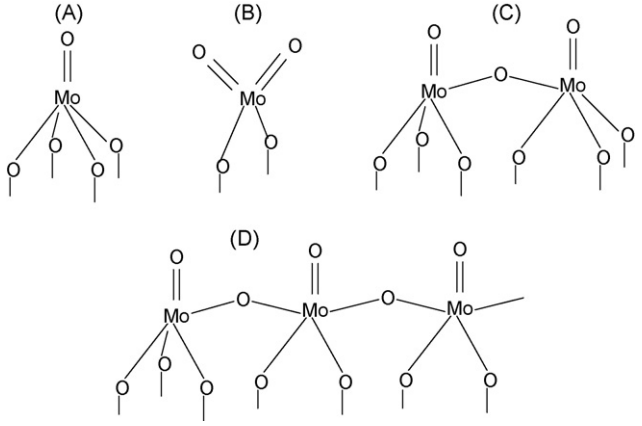

Fig. 3. Possible molecular configurations for MoO_x surface species: (A) di-oxo MoO_4 monomers with distorted tetrahedral coordination; (B) mono-oxo MoO_5 monomers with distorted tetragonal pyramidal coordination; (C) dimeric surface species with distorted octahedral coordination (CN = 5); (D) polymeric MoO_x species.

with a configuration of a tetragonal pyramid (Fig. 3A) in agreement with previous reports [15,16]. The assignment of the 1004 cm^{-1} band is in analogy with the 1008 cm^{-1} Mo=O band of O=$MoC1_4$ [23]. The bands at 988–996 and 840 cm^{-1} (gradually dominating with increasing n_s) are assigned to terminal Mo=O and Mo–O–Mo functionalities of surface polymolybdates. The prevalence of the polymolybdate bands indicates an increasing ratio of polymer-to-monomer populations on the surface. Distorted octahedral configurations with penta-coordinated (MoO_5) (Fig. 3C and D) Mo atom have been proposed for the surface polymolybdates [16,17]. The gradual blue shift of the terminal Mo=O with increasing n_s has been attributed to gradual polymolybdate domain growth [16]. It should be noticed that an increase in the Mo=O bond order would result in a concurrent decrease of the Mo–O(–Zr) bond strength, based in the valence sum rule.

The structure of dispersed molybdena species on TiO_2 (anatase) support is far from being unambiguously resolved [15]. Fig. 2 shows the *in situ* Raman spectra obtained for MoO_3/TiO_2 catalysts under O_2 flow at 450 °C (spectra a–f) and includes the spectrum of crystalline MoO_3 for comparison (spectrum g). For samples with molybdena loadings corresponding to coverage not exceeding the monolayer (spectra a–d of samples with n_s up to 5.8 Mo/nm^2) the spectra are normalised with respect to the strong 630 cm^{-1} TiO_2(anatase) band. This is done in order to illustrate the increase in the relative intensity of bands due to dispersed MoO_x species as compared to the TiO_2 band intensity. A well defined band (observed in the Mo=O stretching region) is seen at 997 cm^{-1} with a tendency for a red shift with increasing loading (994 cm^{-1} in spectrum d, Fig. 2). This band has an asymmetric character implying a low frequency weak component already from spectrum Fig. 2a obtained for the sample with n_s of 1.4 Mo/nm^2. With increasing loading, a broad feature (observed in the Mo–O–Mo region) becomes visible, located at 900–930 cm^{-1}, indicating a partial association of surface MoO_x and formation of polymolybdates. Contrary to the case of MoO_3/ZrO_2 (Fig. 1) and MoO_3/Al_2O_3 [11] the 900–930 cm^{-1} band due to Mo–O–Mo functionalities does not dominate at monolayer loading, indicating a low extent of surface association between MoO_x units on TiO_2. In spectra Fig. 2e and f obtained for samples with n_s of 8.9 and 18.5 Mo/nm^2 the characteristic bands due to MoO_3 bulk crystalline phase become dominant. The asterisks in spectra Fig. 2c and d mark a band indicating the presence of traces of MoO_3 nanoparticles (not detected by XRD) that are dispersed on the surface following few ethane ODH reaction cycles. The spectra in Fig. 2 are in agreement with the ones reported in Ref. [18]. The non-monotonic increase of the S_{BET} for the *x*MoTi samples at low loadings is briefly discussed below. The surface area of TiO_2(anatase) is known to be reduced upon calcination. Often, the incorporation of dispersed species in interstitial sites of the TiO_2 matrix results in a ''resistance'' to the ''collapse'' of measured S_{BET} [24] and this apparently results in the observed initial moderate increase of S_{BET} versus n_s at loadings below monolayer. At loadings exceeding monolayer the surface area is lowered due to formation of crystalline phases. The relatively low value for S_{BET} measured for the 9MoTi sample (Table 1) is attributed to sintering of MoO_3 crystalline nanoparticles for this sample as seen in Fig. 2c.

Our starting point for assignments concerning the isolated species can be the fact that mononuclear oxomolybdenum model compounds possess either a dioxo (O=)$_2MoX_2$ (CN = 4; e.g. O_2MoBr_2 [23]) or a monooxo O = MoX_4 (CN = 5; e.g. O = $MoCl_4$, O = MoF_4 [23]) configuration. Dioxo transition metal–oxygen units possess symmetric (strong) and antisymmetric (weak) M=O Raman modes, the splitting of which is in the 10–30 cm^{-1} range [23,25]. The lack of symmetry in the 994 cm^{-1} is indicative of such overlapping symmetric and antisymmetric Mo=O modes in tetracoordinated (O=)$_2$Mo(–O–)$_2$ (Fig. 3B) and is reminiscent of the respective behaviour in MoO_3/Al_2O_3 catalysts [11]. This picture complements well with the XANES evidence for tetrahedral configuration for surface MoO_x on TiO_2 at low loadings, which gradually transforms into distorted octahedral at high loadings [18], most probably due to association of surface MoO_x into polymeric chains (Fig. 3C and D). Unambiguous differentiation between the monooxo and dioxo configuration for the surface dispersed isolated molybdena species on TiO_2 can be drawn by means of $^{18}O_2$ isotopic substitution experiments, which are in progress.

Fig. 4 shows the *in situ* Raman spectra of monolayer MoO_3/M_xO_y catalysts [(a) 15MoAl; (b) 5.5MoZr; (c) 15MoTi; (d)

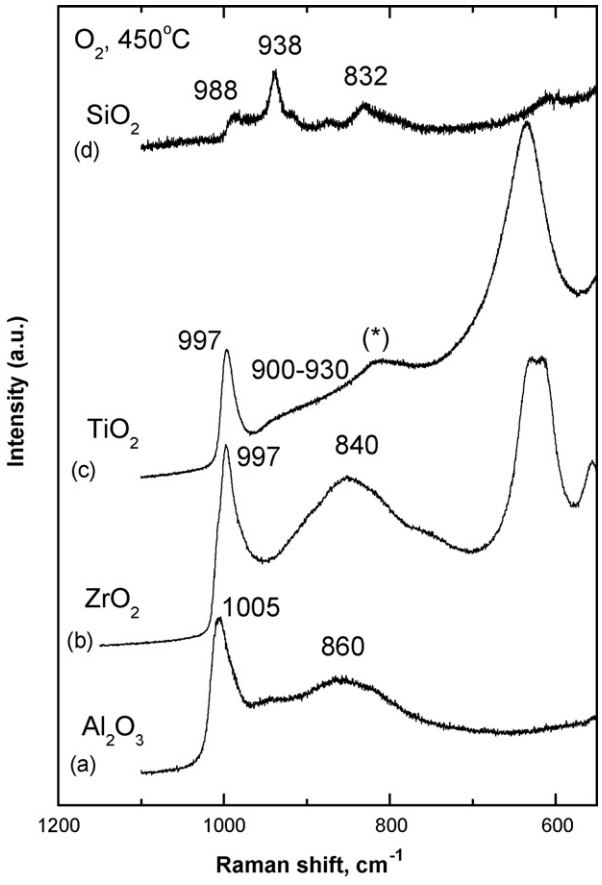

Fig. 4. *In situ* Raman spectra of monolayer MoO_3 catalysts obtained under flowing O_2 at 450 °C: (a) 15MoAl; (b) 5.5MoZr; (c) 15MoTi; (d) 2MoSi. Laser wavelength, λ_0 = 488.0 nm (MoAl and MoZr), λ_0 = 514.5 nm (MoAl and MoZr); recording parameters: see Fig. 1 caption.

Table 2
Summary of observed Raman wavenumbers and proposed structures for dispersed molybdenum oxide on oxide supports in dehydrated conditions

Catalyst	Low coverage ($n_s < 1.7$ Mo/nm^2)			High coverage (approximate monolayer[a])		
	Mo=O (cm^{-1})	Mo–O–Mo (cm^{-1})	Possible structures	Mo=O (cm^{-1})	Mo–O–Mo (cm^{-1})	Possible structures
MoO_3/Al_2O_3[b]	996	850	Isolated, CN = 4 (dioxo); polymolybdate, CN = 5	1005	865	Polymolybdates, CN = 5
MoO_3/ZrO_2	1004, 988	820–840	Isolated, CN = 5 (monooxo); polymolybdate, CN = 5	997	840	Polymolybdates, CN = 5
MoO_3/TiO_2	997		Isolated, CN = 4(?) (dioxo?)	994	900–930	Isolated, CN = 4(?) (dioxo?); polymolybdates, CN = 5
MoO_3/SiO_2[c]	938/920, 988	830, 875				

[a] In the range n_s = 5–6 Mo/nm^2 except for MoO_3/SiO_2 where monolayer is exceeded at $n_s > \sim 1$ Mo/nm^2.
[b] Ref. [11].
[c] Bands assigned tentatively.

2MoSi] obtained at 450 °C under flowing O_2. As seen in Fig. 4, the spectra shown do not exhibit features due to bulk crystalline phases. Table 2 summarises the observed Raman frequencies for the surface isolated and associated (polymeric) MoO_x units, together with proposed coordinations/configurations based on the preceding discussion and findings reported in Ref. [11]. For the case of the catalysts supported on SiO_2, it should be pointed out that the spectra of samples with submonolayer coverage (1MoSi, 2MoSi) exhibit features which are dependent both on loading and temperature (not shown for brevity), indicating the existence of at least two kinds of species (see Fig. 4d and Table 2). Therefore, as pointed out earlier [18,26] the structure of the dispersed MoO_x species on SiO_2 is disputable.

3.3. Catalytic activity and selectivity

The present section will address the catalytic properties of monolayer MoO_3 catalysts supported on Al_2O_3, ZrO_2, TiO_2 and SiO_2 for the ODH of ethane with a view to highlight the effect of the support material. Fig. 5 shows the dependence of ethane conversion areal rate on temperature (in the range 420–540 °C) at a fixed reactant residence time, W/F = 0.28 g s/cm^3, for the samples 5.5MoZr, 15MoAl, 15MoTi and 2MoSi. The rates are normalised per m^2 of catalyst surface area (expressed in μmol C_2H_6 converted/m^2 s) and increase with reaction temperature. Furthermore, the areal rates increase in the order MoSi < MoTi < MoAl < MoZr and the observed differences appear more significant at high temperature. Analogous differences have been observed in previous studies exploring support effects in activities of supported V_2O_5 catalysts for the ODH of C_2–C_3 alkanes [3,5,27] and for the methanol oxidation reaction [28], where differences in reactivities per V site (turnover frequency, TOF) approached even three orders of magnitude [28]; such differences may be accounted for by the much higher intrinsic activity of V based catalysts compared to Mo based catalysts. The dependence of catalyst activity on the support material is less severe for MoO_3 based catalysts as shown in relevant comparative studies for the CH_3OH oxidation reaction [28,29]. In one case, comparing activities between Mo based catalysts supported on Al_2O_3 and TiO_2 for the ODH of ethane it was found that the TiO_2 supported sample had slightly higher activity compared to the Al_2O_3 supported sample [3], contrary to the trends shown in Fig. 5.

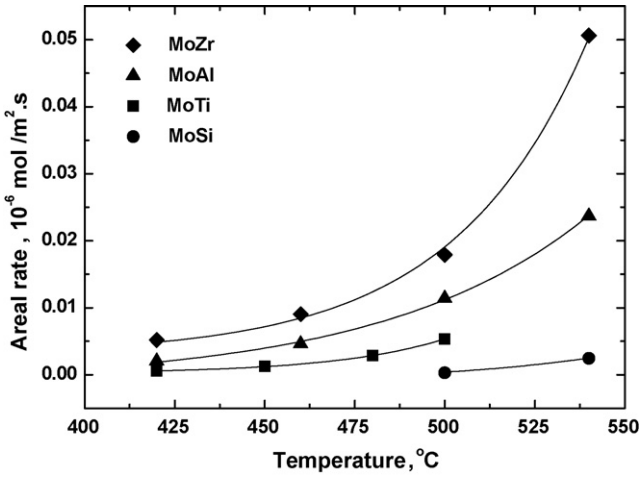

Fig. 5. Ethane conversion areal rate as a function of temperature for supported monolayer MoO_3 catalysts on oxide supports as indicated in the legend. W/F = 0.28 g s/cm^3.

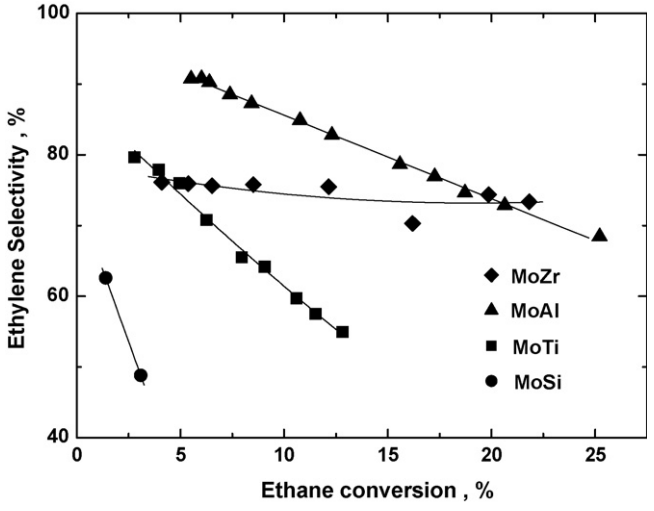

Fig. 6. Ethylene selectivity as a function of ethane conversion for supported monolayer MoO_3 catalysts on oxide supports as indicated in the legend. T = 500 °C.

Initial rates of ODH of C_2–C_3 alkanes (i.e. at low conversions) over supported metal oxides (e.g. V_2O_5, MoO_3) are commonly associated with high olefin selectivities. However, the respective products of the ODH reaction (C_2H_4, C_3H_6) are often involved in secondary activation on the catalyst surface leading to combustion products, CO_x, before leaving the reactor. Such undesired reaction paths are unfortunately more common at high conversions [3,5,11]. Thus, achieving high selectivities at significant conversion levels is of paramount importance and remains a challenge for the design of efficient catalysts for the ODH of light alkanes.

The effect of the oxide support material on C_2H_4 selectivity was examined for each catalyst sample studied by varying the reactants residence time (W/F) in the range 0.05–1 g s/cm^3, in order to achieve various levels of ethane conversion within the range of conditions for differential operation of the reactor in the temperature range 420–540 °C. Fig. 6 shows comparative results of C_2H_4 selectivity as a function of the ethane conversions achieved for the four monolayer MoO_3 catalysts at 500 °C. A poor catalytic behaviour is exhibited by the SiO_2 supported sample, whereas significant C_2H_4 selectivity levels are attained for the Al_2O_3, ZrO_2 and TiO_2 supported samples. The MoAl sample has the highest selectivity at low conversions, while the MoTi sample exhibits a steep drop of selectivity with increasing conversion. The MoZr sample sows a remarkable stability as far as the dependence of its selectivity versus conversion is concerned; remarkably it is the most selective catalyst at high conversions.

Comparative assessments of catalyst reactivity can be made on the basis of the turnover frequency (TOF, rate of ethane consumption per Mo site) which reflects both the site reactivity and site availability/accessibility. This information can be complemented by comparing the apparent activation energies obtained from Arrhenius plots of ln TOF versus 1/T. Fig. 7 shows the Arrhenius-type plots obtained for MoO_3 catalysts supported on the four different oxide supports with approximate monolayer composition, based on data from differential reactor operation at constant reactant residence time, W/F = 0.28 g s/cm^3. At all temperatures the TOFs observed increase in the order MoZr > MoAl > MoTi > MoSi and the apparent activation energies, E_a, calculated from the slopes of the lines in Fig. 7 exhibit an inverse trend: E_a (MoZr) = 88 kJ/mol < E_a (MoAl) = 97 kJ/mol < E_a (MoTi) = 125 kJ/mol < E_a (MoSi) = 278 kJ/mol. The last value concerning the MoSi sample should be considered with caution, since it is based only on two measurement points. The inverse trend exhibited by the E_a values compared to the trends in TOFs is not surprising; the higher the catalyst reactivity, the higher the ability for activation of the C–H bond and the lower the activation energy for this step.

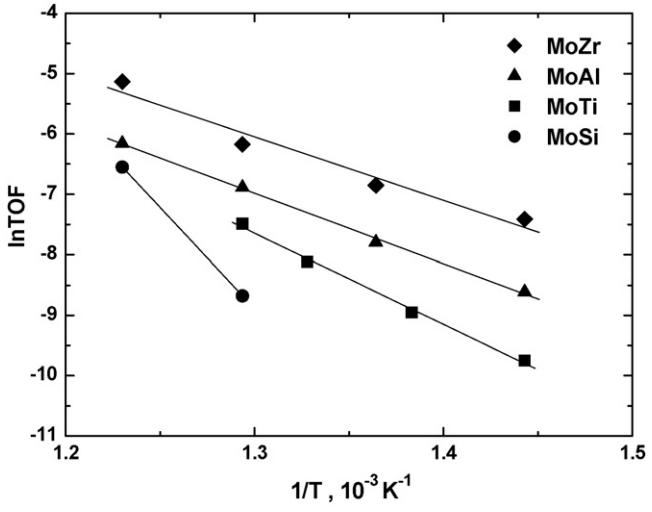

Fig. 7. Arrhenius plots for supported monolayer MoO_3 catalysts on oxide supports as indicated in the legend.

It is noteworthy that the qualitative and quantitative results and trends obtained when comparing the performance of catalysts with similar surface density (n_s = 3.8–3.9 Mo/nm^2, i.e. 4MoZr, 15MoAl, 9MoTi and 7MoSi) are similar to the ones shown in Figs. 5–7 (not shown for brevity).

3.4. Highlighting the support effect

In the literature, there is a consensus that the alkane ODH reactions over supported metal oxides proceed via a Mars–van Krevelen redox type mechanism involving lattice oxygen [8]. However, the nature of the particular oxygen site involved in the C–H bond activation is under debate. In the present study, focusing on the catalytic properties of MoO_3 catalysts supported in various oxide supports with coverages corresponding to a monolayer, the surface composition incorporates dispersed MoO_x units in isolated (monomeric) and/or associated (polymeric) form including in particular: (i) isolated MoO_4 and MoO_5 units (A and B in Fig. 3) and (ii) associated (polymeric) units (C and D in Fig. 3). Thus, the various comparative assessments of catalyst performance for the ODH of ethane are likely to depend on the critical oxygen site that could in principle be involved in Mo=O terminal bonds, Mo–O–Mo bridging bonds connecting associated MoO_x units or Mo–O–M (M = Zr, Al, Ti and Si) anchoring bonds of dispersed surface species. Therefore the observed differences can be neither due to effects of vacant support sites (as such sites do not exist) nor to properties of bulk phases, because the coverage is at approximate monolayer. Previously, M=O centers (M=V, Mo) were not considered of importance for methanol oxidation and ethane ODH reactions over MoO_3/Al_2O_3 catalysts [11,29,30] and for propane ODH over V_2O_5/TiO_2 and V_2O_5/ZrO_2 catalysts [5,31], although in one case it has been reported that Mo=O bonds are involved in C–H bond activation for the ODH of propane over MoO_3/ZrO_2 catalysts [9]. Moreover, it is unlikely that the oxygen involved in bridging Mo–O–Mo bonds is involved in C–H bond activation, because the similarity of the structural configurations between the associated (polymeric) MoO_x species (which are predominant at monolayer coverage at least on ZrO_2 and Al_2O_3) on the various supports cannot justify the observed differences in catalyst performance (Figs. 5–7). For example, the surface composition of monolayer MoZr and MoAl catalysts is quite similar, consisted of polymolybdates with distorted octahedral pentacoordinated Mo

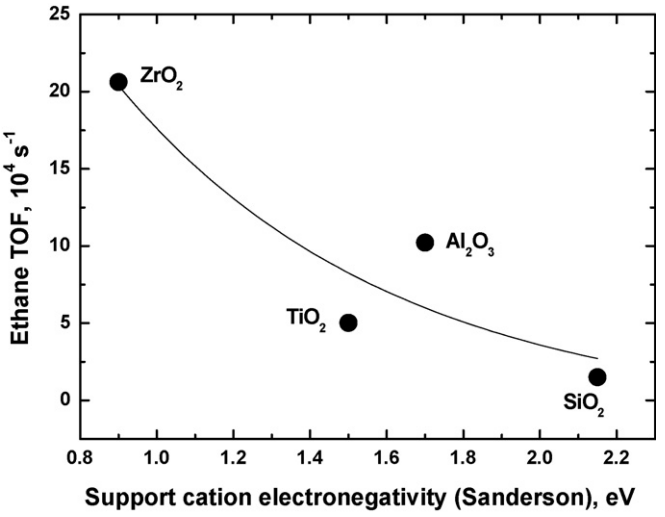

Fig. 8. Steady-state ethane turnover frequency for supported monolayer MoO_3 catalysts as a function of support cation electronegativity. $T = 500\ ^\circ C$; $W/F = 0.28$ g s/cm^3.

with comparable strengths involved in the respective bonds within their Mo=O and Mo–O–Mo functionalities. To the contrary, the importance of Mo–O–support anchoring bonds has been demonstrated for catalytic oxidation reactions over supported metal oxide catalysts [29,31]. Furthermore, the importance of Mo–O–support bonds for propane and ethane ODH has been demonstrated based on concurrent trends of the activity per site (V and Mo) and the number of anchoring bonds per site (V and Mo) as a function of surface density, n_s [5,11].

A systematic study of the support effect on the catalytic activity of V_2O_5-based catalysts for the CH_3OH oxidation reaction has led to the establishment of a trend according to which there is an inverse correlation between the steady-state catalytic TOF and the support cation electronegativity ([32] and references therein). Such a correlation has been found also in the present work. Fig. 8 shows the steady-state ethane TOF measured at 500 °C for the supported MoO_3 catalysts with approximate monolayer coverage for reactants residence time $W/F = 0.28$ g s/cm^3 plotted versus the support cation electronegativity. Therefore, it turns out that the influence of the support is manifested most probably by means of a ligand effect mechanism connected to the support cation electronegativity. A low support cation electronegativity results in increased electron density (basicity) of the oxygen site involved in the Mo–O–M anchoring bond, thereby increasing its activity for redox processes. Obviously, the correlation in Fig. 8 is not perfect and this could be due to the fact that the catalytic activity is not solely controlled by the active site reactivity but also from factors related to site availability/accessibility as well as the possible active phase heterogeneity, e.g. the occurrence of active sites in isolated or associated (polymeric) MoO_x units with different Mo–O bond orders along Mo–O–support anchoring bridges and/or different numbers of Mo–O–support bonds per Mo [5,11] depending on the structural configuration of the dispersed MoO_x species (Fig. 3).

4. Conclusion

The Raman spectra of MoO_3 catalysts supported on ZrO_2, Al_2O_3, TiO_2 and SiO_2 recorded under O_2 show the existence of surface dispersed molybdena species in various configurations, which are dependent on loading and/or temperature. At low loadings, isolated (monomeric) MoO_x species prevail on the surface with the Mo atom being either in monooxo configuration with CN = 5(MoO_3/ZrO_2) or dioxo configuration with CN = 4(MoO_3/Al_2O_3 and probably MoO_3/TiO_2); at higher loadings, incorporation of Mo to Mo–O–Mo bridges results in the occurrence of associated MoO_x units in the form of polymeric chains with the Mo atom in distorted octahedral-like configuration with CN = 5. Bulk crystalline phases are formed on the support surfaces when loading exceeds monolayer coverage. Increased relative amounts of surface isolated MoO_x species are found on TiO_2 at monolayer coverage, compared to ZrO_2 and Al_2O_3 where associated MoO_x units in the form of polymeric chains prevail at monolayer loadings. The nature of the oxide support material and of the Mo–O–support bond has a significant influence on the catalytic behaviour of the molybdena catalysts with monolayer coverage studied for the ODH of ethane. The dependence of reactivity on the support follows the order $ZrO_2 > Al_2O_3 > TiO_2 > SiO_2$, whereas the respective activation energies follow the inverse order E_a (ZrO_2) < E_a (Al_2O_3) < E_a (TiO_2) < E_a (SiO_2), i.e. high catalyst reactivity is associated with easier C–H bond activation. The steady-state ethane TOF values appear to be inversely correlated to the support cation electronegativities.

Acknowledgements

The authors are grateful to P. Tsourapas for undertaking a part of the experimental work and to Angeliki Lemonidou and Eleni Heracleous (University of Thessaloniki) for providing the MoAl catalyst samples. Financial support from the European Social Fund (ESF), Operational Program for Educational and Vocational Training II (EPEAEK II), and particularly the HRAKLEITOS program is gratefully acknowledged.

References

[1] A.M. Beale, A.M.J. van der Eerden, K. Kervinen, M.A. Newton, B.M. Weckhuysen, Chem. Commun. (2005) 3015.
[2] E.A. Mamedov, V.C. Corberán, Appl. Catal. A 127 (1995) 1.
[3] E. Heracleous, M. Machli, A.A. Lemonidou, I.A. Vasalos, J. Mol. Catal. A: Chem. 232 (2005) 29.
[4] K. Chen, A.T. Bell, E. Iglesia, J. Catal. 209 (2002) 35.
[5] A. Christodoulakis, M. Machli, A.A. Lemonidou, S. Boghosian, J. Catal. 222 (2004) 293.
[6] E. Heracleous, A.F. Lee, I.A. Vasalos, A.A. Lemonidou, Catal. Lett. 88 (2003) 47.
[7] M.C. Abello, M.F. Gomez, O. Ferretti, Appl. Catal. A: Gen. 207 (2001) 421.
[8] K. Chen, A.T. Bell, E. Iglesia, J. Phys. Chem. B 104 (2000) 1292.
[9] K. Chen, S. Xie, E. Iglesia, A.T. Bell, J. Catal. 189 (2000) 421.
[10] E. Heracleous, J. Vakros, A.A. Lemonidou, Ch. Kordulis, Catal. Today 91–92 (2004) 289.
[11] A. Christodoulakis, E. Heracleous, A.A. Lemonidou, S. Boghosian, J. Catal. 242 (2006) 16.

[12] I.E. Wachs, Catal. Today 27 (1996) 437.
[13] G. Mestl, J. Mol. Catal. A: Chem. 158 (2000) 45.
[14] I.E. Wachs, Top. Catal. 8 (1999) 57.
[15] G. Mestl, T.K.K. Srinivasan, Catal. Rev. Sci. Eng. 40 (4) (1998) 451.
[16] S. Xie, K. Chen, A.T. Bell, E. Iglesia, J. Phys. Chem. B 104 (2000) 10059.
[17] B.M. Weckhuysen, J.-M. Jehng, I.E. Wachs, J. Phys. Chem. B 104 (2000) 7382.
[18] H. Hu, I.E. Wachs, S.R. Bare, J. Phys. Chem. 99 (1995) 10897.
[19] B.M. Weckhuysen, Chem. Commun. (2002) 97.
[20] C.G. Cortez, M.A. Banares, J. Catal. 209 (2002) 197.
[21] J.C. Edwards, R.D. Adams, P.D. Ellis, J. Am. Chem. Soc. 112 (1990) 8349.
[22] Y. Matsuoka, M. Niwa, Y. Murakami, J. Phys. Chem. 94 (1990) 1477.
[23] K. Nakamoto, Infrared and Raman Spectra of Inorganic and Coordination Compounds, 4th ed., Wiley–Interscience, New York, 1986.
[24] T.I. Halkides, D.I. Kondarides, X.E. Verykios, Appl. Catal. B: Environ. 41 (2003) 415.
[25] G. Busca, J. Raman Spectrosc. 33 (2002) 348.
[26] N. Ohler, A.T. Bell, J. Catal. 231 (2005) 115.
[27] A. Khodakov, B. Olthof, A.T. Bell, E. Iglesia, J. Catal. 181 (1999) 205.
[28] L.J. Burcham, M. Badlani, I.E. Wachs, J. Catal. 203 (2001) 104.
[29] D.S. Kim, I.E. Wachs, K. Segawa, J. Catal. 146 (1994) 268.
[30] H. Hu, I.E. Wachs, J. Phys. Chem. 99 (1995) 10911.
[31] B.M. Weckhuysen, D.E. Keller, Catal. Today 78 (2003) 25.
[32] I.E. Wachs, Catal. Today 100 (2005) 79.